DALTON
FULL PAPER

Syntheses, structures and magnetism of α-$Mn(dca)_2$, $[Mn(dca)_2(H_2O)_2]\cdot H_2O$, $[Mn(dca)_2(C_2H_5OH)_2]\cdot(CH_3)_2CO$, $[Fe(dca)_2(CH_3OH)_2]$ and $[Mn(dca)_2(L)_2]$, where L = pyridine, CH_3OH or DMF and $dca^- = dicyanamide$, $N(CN)_2^-$ †

Stuart R. Batten,[a] Paul Jensen,[a] Cameron J. Kepert,[b] Mohamedally Kurmoo,*[c] Boujemaa Moubaraki,[a] Keith S. Murray*[a] and David J. Price[a]

[a] *Chemistry Department, Monash University, Clayton, Victoria 3168, Australia. Fax: +613 9905 4597; E-mail: Keith.S.Murray@sci.monash.edu.au*
[b] *Inorganic Chemistry Laboratory, South Parks Road, Oxford, UK OX1 3QR*
[c] *Institut de Physique et Chimie des Matériaux de Strasbourg (GMI), CNRS-UMR 7504, 23 rue du Loess, F-67037 Strasbourg Cedex, France*

Received 4th May 1999, Accepted 6th July 1999

The dicyanamide anion has been observed to adopt two bridging co-ordination modes (μ and μ_3) in α-$Mn(dca)_2$, $[Mn(dca)_2(H_2O)_2]\cdot H_2O$, $[Mn(dca)_2(C_2H_5OH)_2]\cdot(CH_3)_2CO$, $[Fe(dca)_2(CH_3OH)_2]$ and $[Mn(dca)_2(L)_2]$ [L = py, CH_3OH or DMF; dca = dycanamide $N(CN)_2^-$], and generates weak ligand fields thus stabilising high spin configurations. The N- or O-bonded ligands L play an important role in the stabilisation of both the molecular structures and the three dimensional structure, *via* hydrogen bonding. The unsolvated α-$Mn(dca)_2$ adopts a rutile-like single network structure, based on the near orthogonal packing of 'ribbons' of . . . $Mn(N{\equiv}C{-}N{-}C{\equiv}N)_2Mn$ . . ., similar to that found for the isomorphous analogues of Co, Ni, Fe and Cu. Magnetisation measurements confirmed a high spin manganese d^5 system displaying antiferromagnetic coupling ($\theta = -25$ K) above 25 K and undergoing long range magnetic ordering ($T_N = 16$ K) to a spin-canted antiferromagnet (weak ferromagnet). Magnetisation and heat capacity measurements on some samples of α-$Mn(dca)_2$ indicated a possible second transition at ≈6 K, the nature of which is under investigation. From the hysteresis data at 2 K (remnant magnetisation of 29 cm^3 Oe mol^{-1} and coercive field of 406 Oe) a canting angle of 0.05° is estimated for this soft magnet. Other samples gave a higher value for the coercive field. The α-$M(dca)_2$ series has a diverse range of ground states; Cu^{II} (d^9) is a paramagnet, Ni^{II} (d^8) and Co^{II} (d^7) are ferromagnets and Fe^{II} (d^6) and Mn^{II} (d^5) are canted antiferromagnets. Reasons for this diversity are given on the basis of the nature of exchange coupling pathways within the rutile structure and a mechanism for the long range magnetic ordering is proposed. A range of 1-D chain complexes of type $[Mn(dca)_2(L)_2]$, containing 'ribbons' of doubly bridged $Mn(N{\equiv}C{-}N{-}C{\equiv}N)_2Mn$ have been structurally characterised. The complex $[Fe(dca)_2(CH_3OH)_2]$ is isostructural with the manganese analogue. 2-D Square grids are found in crystals of $[Mn(dca)_2(C_2H_5OH)_2]\cdot(CH_3)_2CO$ and in $[Mn(dca)_2(H_2O)_2]\cdot H_2O$, the latter displaying, in addition, penetration of ribbons of *trans*-$Mn(dca)_2(H_2O)_2$ through the grids. Dehydration or desolvation results in formation of the α-$Mn(dca)_2$ phase. The Lewis-base adducts all display very weak antiferromagnetic coupling ($J \approx -0.12$ cm^{-1}) and no magnetic long-range order. Dissolution of the compounds in protic solvents leads to complete dissociation of the dicyanamide, and the axially co-ordinated ligands, L, can readily be exchanged by reaction or recrystallisation in different co-ordinating solvents.

Recently we have independently described[1,2] details of the structural and physical properties of a series of magnetic dicyanamide–d block binary compounds of the type $M^{II}(dca)_2$, where M^{II} = Co, Ni, Fe, Mn or Cu and $dca^- = N(CN)_2^-$. One of the features of the dicyanamide anion is its weak ligand field relative to the cyanide anion thus stabilising high spin states. Most important is the range of co-ordination modes this ligand can adopt in its chemistry compared to only one for the well studied cyanide ligand. The latter is known to stabilise interesting 3-D magnetic structures with differing ground states depending on the spin states of the metals and on the vacancies within the cubic Prussian blue structure.[3,4] Transition temperatures that exceed room temperature have been noted in a few Prussian blue analogues.[5] The isostructural series, labelled α-$M(dca)_2$, adopts a rutile-like single network structure containing . . . $M(N{\equiv}C{-}N{-}C{\equiv}N)_2M$ . . . ribbons of metal ions bridged by two dca^- moieties *via* their nitrile N donor atoms. Six-co-ordination of donor atoms around the metal(II) ion is achieved through bridging to adjacent chains *via* the amide N donor atoms. In the case of Cu^{II}, the Cu–N (amide) bond lengths are greater than are the Cu–N (nitrile) lengths because of Jahn–Teller effects. The series also displays an intriguing set of magnetic properties, *viz*. the copper(II) compound behaves as a near paramagnet whilst the compounds of Co^{II} and Ni^{II} are new examples of homometallic ferromagnets with T_c values, respectively, of 9 and 21 K. The iron(II) derivative has the characteristics of a canted antiferromagnet. Detailed physical studies of these magnets have been made.[2,6] In a recent paper, Manson *et al.*[7] have confirmed our initial observations[1,2] on the derivatives of Co and Ni. In the present paper we describe the occurrence of long-range magnetic ordering in the antiferromagnetically coupled manganese(II) analogue, α-$Mn(dca)_2$. It is

† *Supplementary data available*: hydrogen bonding interactions, atom numbering schemes. For direct electronic access see http://www.rsc.org/suppdata/dt/1999/2987/, otherwise available from BLDSC (No. SUP 57610, 4 pp.) or the RSC Library. See Instructions for Authors, 1999, Issue 1 (http://www.rsc.org/dalton).

a new example of a rapidly growing class of homometallic spin-canted antiferromagnets (weak ferromagnets).

Following these observations, we have embarked on the study of co-ordination complexes where monodentate ligands (L)[2] and bidentate (LL)[8,9] are used to block the fifth and sixth co-ordination sites of the basic ribbons . . . $M(N{\equiv}C–N–C{\equiv}N)_2M$ . . . to create low dimensional quantum magnetic systems. A much sought after system is a Haldane chain having $S = 2$ centres; only one manganese(III) example has been described.[10] A possible derivative based on the structural data on the present set of compounds would be $Fe^{II}(dca)_2L_2$ and we include here structural data on the $L = CH_3OH$ adduct.[11] We also describe the structures and magnetism of a wide range of chain compounds of type $[Mn(dca)_2(L)_2]$, where $L = CH_3OH$, pyridine (py) or dimethylformamide (DMF) and of square-grid sheet systems found in $[Mn(dca)_2(C_2H_5OH)_2]\cdot(CH_3)_2CO$ and in $[Mn(dca)_2(H_2O)_2]\cdot H_2O$, the latter being a second crystalline phase obtained during synthesis of $Mn(dca)_2$ from water. Some unusual solid state transformations occur when the ligand (L) is removed. In particular, removal of water from $[Mn(dca)_2(H_2O)_2]\cdot H_2O$ gives back α-$Mn(dca)_2$ with similar magnetic properties to those of the parent compound, the corresponding structural transformation involving Mn to dca bond breaking and bond forming processes. Preliminary data have been communicated.[12] We note that the pioneering work on metal-dicyanamide co-ordination- and magneto-chemistry by Köhler and Hvastijová, and colleagues has emphasised chain-like $[M(dca)_2(L)_2]$ species, where L = pyridine or imidazole bases, and M^{II} = Co, Ni or Cu, but crystal structures have generally been lacking.[13] Based on our own experiences and those of ref. 13 we may conclude that the rich chemistry of the manganese dicyanamide presented here compared to those of Co, Ni and Cu is due principally to the solubility of the manganese products and the ease of recrystallisation.

Experimental

Syntheses

α-$Mn(dca)_2$. *Method 1.* The compounds $Mn(ClO_4)_2\cdot 6H_2O$ (1.81 g, 5.0 mmol) and Na(dca) (0.89 g, 10.0 mmol) were dissolved in 30 cm^3 of water. The solution was heated to 80 °C for 1 h. Slow evaporation over 2 d gave very pale blue triangular prismatic crystals that were filtered off and washed with small quantities of cold ethanol and diethyl ether and dried in air. Yield 0.38 g, 40%. Found: C, 25.8; H, 0; N, 45.1. Calc. for C_4MnN_6: C, 25.7; H, 0; N, 44.9%.

Method 2. Water (2 cm^3) was added to a mixture of solid $Mn(ClO_4)_2\cdot 6H_2O$ (1.81 g, 5.0 mmol) and Na(dca) (0.89 g, 10.0 mmol) then heated to boiling for 5 min during which a very pale blue solid formed. The microcrystalline solid was washed thoroughly with ethanol and diethyl ether. Yield 0.46 g, 49%. Found: C, 25.6; H, 0; N, 44.9. Calc. for C_4MnN_6: C, 25.7; H, 0; N, 44.9%. μ_{eff} (289.5 K) = 5.43 μ_B. Λ_M (10^{-3}M in water) = 224 S cm^{-1}. IR (cm^{-1}, Nujol) 2360w, 2325m, 2292s, 2262s and 2192s.

This method is preferred over Method 1 for obtaining solely α-$Mn(dca)_2$; $Mn(NO_3)_2\cdot 6H_2O$ can be used instead of the perchlorate salt. Method 1 often yielded mixtures of blue tinged prismatic α-$Mn(dca)_2$ and colourless cubic crystals of $Mn(dca)_2(H_2O)_2\cdot H_2O$, described below. Each can readily be distinguished by their colours and crystal morphologies.

$[Mn(dca)_2(H_2O)_2]\cdot H_2O$. A hot solution of Na(dca) (0.89 g, 10.0 mmol) in water (15 cm^3) was combined with a hot aqueous solution (10 cm^3) of $Mn(ClO_4)_2\cdot 6H_2O$ (1.81 g, 5.0 mmol) and maintained at 80 °C for 4 h. The solution was left to evaporate for 8 d after which time clusters of very pale blue transparent crystals were present along with individual cube shaped crystals. A quick wash with water of a cluster of the trihydrate crystals gave a sample with microanalytical data as follows. Found: C, 20.1; H, 1.9; N, 34.6. Calc. for $C_4H_6MnN_6O_3$: C, 19.9; H, 2.5; N, 34.9%. IR (cm^{-1}, Nujol) 2301s, 2254s and 2183s. Exposure of crystals of the trihydrate to air for several hours yields an opaque off-white sample of α-$Mn(dca)_2$, characterised by its IR spectral and magnetic properties. Crushing a cluster of crystals of $[Mn(dca)_2(H_2O)_2]\cdot H_2O$ followed by washing sequentially with acetone, ethanol and ether also yielded α-$Mn(dca)_2$.

$[Mn(dca)_2(py)_2]$. A methanolic solution (10 cm^3) of $Mn(ClO_4)_2\cdot 6H_2O$ (1.81 g, 5.0 mmol) was added to a stirred methanolic solution (40 cm^3) of Na(dca) (0.89 g, 10.0 mmol). Pyridine (1.5 cm^3) was added dropwise with stirring, resulting in formation of a fine white precipitate of the pyridine adduct. This dissolved when the solution was diluted to 100 cm^3 and gently heated. On standing for 8 d colourless crystals of the product formed and were washed with ether. Yield 1.07 g, 62%. Found: C, 48.7; H, 2.7; N, 32.8. Calc. for $C_{14}H_{10}MnN_8$: C, 48.7; H, 2.9; N, 32.5% μ_{eff}(292.5 K) = 5.80 μ_B. IR (cm^{-1}, Nujol): 2360w, 2797s, 2236s and 2173s. The crystals are stable in air towards loss of pyridine.

$[Mn(dca)_2(CH_3OH)_2]$. *Method 1.* An ethanolic solution (10 cm^3) of $Mn(ClO_4)_2\cdot 6H_2O$ (1.81 g, 5.0 mmol) was combined with a hot (60 °C) methanolic solution (30 cm^3) of Na(dca) (0.89 g, 10.0 mmol). After standing for 3 d at room temperature crystals of the methanolate complex were formed. They rapidly lose methanol on standing in air and revert to α-$Mn(dca)_2$. Found: C, 28.5; H, 2.9; N, 34.0. Calc. for $C_6H_8MnN_6O_2$: C, 28.7; H, 3.2; N, 33.5%. IR (cm^{-1}, Nujol) 2359w (sh), 2291s, 2253s and 2189s.

Method 2. The methanolate complex could also be obtained by treating $Mn(NO_3)_2\cdot 6H_2O$ with Na(dca) in water followed by addition of methanol and refrigeration at 5 °C for 24 h. Large colourless crystals were obtained.

$[Fe(dca)_2(CH_3OH)_2]$. An attempt at preparing $Fe(dca)_2$ from methanol, involving layering a methanolic solution (20 cm^3) of Na(dca) (0.179 g, 2.0 mmol) over 5 cm^3 layers of methanol, ethanol and an ethanolic solution (10 cm^3) of $Fe(ClO_4)_2\cdot 6H_2O$ (0.365 g, 1.0 mmol), after several weeks yielded a yellow solution with a brown powder at the bottom of the vessel in which a small number of colourless crystals of $[Fe(dca)_2(CH_3OH)_2]$ were found.

$[Mn(dca)_2(C_2H_5OH)_2]\cdot(CH_3)_2CO$. These large colourless crystals were obtained by Method 2, above, employing a mixture of ethanol and acetone instead of methanol. They lose solvent rapidly when exposed to air.

$[Mn(dca)_2((CH_3)_2NCHO)_2]$. The compound $Mn(dca)_2$ (0.100 g) was dissolved in 10 cm^3 of warm dimethylformamide held at 50 °C. After cooling and standing at room temperature for 5 d colourless crystals were formed. They lose solvent slowly in the air. Found: C, 35.7; H, 4.1; N, 33.2. Calc. for $C_{10}H_{14}MnN_8O_2$: C, 36.0; H, 4.2; N, 33.5%. IR (cm^{-1}, Nujol) 2308s, 2235s, 2183s. 1652s [ν(C=O)].

Desolvation studies

(a) Dehydration of $[Mn(dca)_2(H_2O)_2]\cdot H_2O$. A thermogravimetric analysis using a Stanton-Redcroft Thermal Analyser showed the sequential loss of each water molecule. Complete dehydration was carried out by heating a preweighed sample under vacuum, in an electric oven held at 85 °C, with the sample contained in a vial inside a Schlenk tube. Mass loss 23.6% (calc. 22.4%). The IR spectrum and powder XRD pattern of the product was consistent with that of α-$Mn(dca)_2$.

(b) Depyridination of $[Mn(dca)_2(py)_2]$. A 0.2293 g sample of

$Mn(dca)_2(py)_2$ was placed in a pre-weighed vial in a Schlenk tube and heated, under vacuum, in an electric oven at *ca.* 200 °C for 2 d. Final mass 0.1254 g; % mass loss = 45.3, calc. 45.8. The IR spectrum of the resulting $Mn(dca)_2$, kept under a nitrogen atmosphere, was identical to that of the rutile-like α phase and not to the β phase previously reported by Köhler.[14]

X-Ray crystallographic studies

Crystal data are summarised in Table 1. The crystal structure of $[Mn(dca)_2(CH_3OH)_2]$ was determined independently at both Monash University and Oxford, and as both solutions were identical only the Oxford result is presented.

The compounds α-$Mn(dca)_2$, $[Mn(dca)_2(H_2O)_2]\cdot H_2O$, $[Mn(dca)_2(py)_2]$, $[Mn(dca)_2(DMF)_2]$ and $[Fe(dca)_2(CH_3OH)_2]$ were studied at Monash University. Data were collected on a Nonius KappaCCD diffractometer with graphite monochromated Mo-Kα radiation ($\lambda = 0.71073$ Å). Integration was carried out by the program DENZO-SMN,[15] and data were corrected for Lorentz-polarisation effects and for absorption using the program SCALEPACK.[15] Solutions were obtained by direct methods (SHELXS 97)[16] followed by successive Fourier-difference methods, and refined by full matrix least squares on F_{obs}^2 (SHELXL 97).[16] All non-hydrogen atoms were made anisotropic, while all hydrogens (except in the hydrate and the methanolate) were assigned to calculated positions. All the protons in the hydrate and the methanolate were found in the difference maps (except H32 in the hydrate, whose initial position was calculated), and allowed to refine freely.

The compounds $[Mn(dca)_2(CH_3OH)_2]$ and $[Mn(dca)_2(C_2H_5OH)_2]\cdot(CH_3)_2CO$ were studied at the University of Oxford. Single crystal X-ray refinement data were collected on an Enraf-Nonius DIP2000 diffractometer equipped with graphite-monochromated Mo-Kα radiation, a nitrogen gas cryostream and Eu/Ba image plate detectors. Ninety consecutive 2° oscillations in φ performed and the images processed with the HKL suite of programs.[15] Structures were solved by direct methods (SHELXS 86)[17] and refined by full matrix least squares on F_{obs}^2 (SHELXL 93).[18] Hydrogen atoms were located in the difference maps and allowed to refine freely. A table of hydrogen bonding interactions for $[M(dca)_2(CH_3OH)_2]$, M = Mn or Fe, $[Mn(dca)_2(C_2H_5OH)_2]\cdot(CH_3)_2CO$ and $[Mn(dca)_2(H_2O)_2]\cdot H_2O$ are also available as supplementary data (SUP 57610).

CCDC reference number 186/1562.

See http://www.rsc.org/suppdata/dt/1999/2987/ for crystallographic files in .cif format.

Magnetic studies

Investigations at Monash University employed a Quantum Design MPMS 5 SQUID magnetometer calibrated by use of a standard palladium sample (Quantum Design) of accurately known magnetisation or by use of magnetochemical calibrants such as $CuSO_4\cdot 5H_2O$ and $[Ni(en)_3]S_2O_3$. Susceptibility *vs.* temperature studies in the linear portion of the magnetisation *vs.* field curve were made using a field of 1T. Powdered samples were contained in calibrated gelatine capsules held at the centre of a drinking straw fixed to the end of the sample rod. Samples which readily lost solvent molecules were sealed in quartz containers.

Investigations of magnetisation *vs.* temperature with zero-field-cooling (ZFCM), field-cooling (FCM) and remnant magnetisation (RM) were made at Monash University using a field of 5 Oe. Hysteresis measurements were made at the temperatures stated in the text using microcrystalline powders contained in gelatine capsules. The hysteresis loop was also measured with the sample dispersed in Vaseline in order to eliminate any torquing of crystallites. Care was taken to eliminate any remaining field in the magnet prior to measuring the hysteresis loops. Magnetisation *vs.* field (up to 5 T) studies employed powdered samples. Further hysteresis measurements were performed in Strasbourg using a vibrating sample magnetometer model PAR155 with a maximum field of 1.8 T. The temperature was controlled by a helium bath cryostat and an Oxford Instruments temperature controller ITC4. Samples were held tightly in a Delrin container to eliminate torquing effects. For fields greater than 1.8 T a Quantum Design MPMS instrument was used for hysteresis on a powdered sample.

The heat capacity of α-$Mn(dca)_2$ was measured at Strasbourg on a 250 mg sample pressed in to a 5 mm diameter pellet by a pseudo-adiabatic method as described previously.[2] AC Susceptibilities (χ' and χ'') were measured in Strasbourg using a Quantum Design MPMS SQUID magnetometer with $H_{AC} = 1$ Oe oscillating at 20 Hz. Confirmatory DC magnetisation measurements were also made at Strasbourg using the MPMS SQUID instruments in fields of 0.1 and 3 Oe, at temperatures down to 1.8 K.

Results and discussion

Synthesis and characterisation

The complexes α-$Mn(dca)_2$ and $[Mn(dca)_2(H_2O)_2]\cdot H_2O$ both crystallise out of concentrated aqueous solutions containing predissolved $Mn(ClO_4)_2\cdot 6H_2O$ and sodium dicyanamide mixed in a 1 : 2 mole ratio. The $Mn(dca)_2$ crystals are triangular prismatic in habit whilst $[Mn(dca)_2(H_2O)_2]\cdot H_2O$ crystals appear almost cubic. They were readily separated by hand. The trihydrate could be obtained as the sole product by redissolving the mixture of crystals and allowing slow evaporation. The molar conductivity value for $Mn(dca)_2$ in water is typical of a 1 : 2 electrolyte (224 S cm^{-1}), suggesting that the ligands dissociate in solution and reassociate upon crystallisation of the monoclinic trihydrate phase. To get α-$Mn(dca)_2$ alone, a mixture of solid $Mn(ClO_4)_2\cdot 6H_2O$ and Na(dca) was dissolved in the minimum amount of water, the product crystallising rapidly upon warming, before being washed with ethanol and diethyl ether. These compounds, and the other Lewis-base adducts described below, were identified by their XRD patterns and by infrared spectroscopy, the key dca bands being listed in the Experimental section.

The complex $[Mn(dca)_2(CH_3OH)_2]$ was prepared either by adding methanol to an aqueous solution of $Mn(dca)_2$ or by mixing a methanolic solution of ligand with an ethanolic solution of $Mn(ClO_4)_2\cdot 6H_2O$; $[Fe(dca)_2(CH_3OH)_2]$ was prepared likewise but was contaminated with other products. When absolute ethanol was used as solvent in the latter case α-$Fe(dca)_2$ was obtained.[2] Thus co-ordination of methanol rather than water or ethanol is preferred in these crystallisations. The ethanolate derivative of $Mn(dca)_2$ was obtained by adding a mixture of ethanol and acetone rather than methanol to the aqueous solution. The DMF adduct was obtained by dissolving $Mn(dca)_2$ in DMF. All these O-bonded solvated species lose the co-ordinated water, alcohol or DMF, at varying rates, upon exposure to air. Careful dehydration of $[Mn(dca)_2(H_2O)_2]\cdot H_2O$ yielded α-$Mn(dca)_2$, a somewhat surprising process which involves bond breaking and bond forming.

The pyridine adduct, $[Mn(dca)_2(py)_2]$, was obtained by addition of pyridine to a methanolic solution of $Mn(ClO_4)_2\cdot 6H_2O$ and Na(dca). It is stable in air and can be depyridinated to yield α-$Mn(dca)_2$ by heating under vacuum.

Structures

The dicyanamide anion is a remarkably versatile building block for the construction of supramolecular architectures. It forms strong covalent bonds and usually acts as a uni-, bi- or tridentate ligand.[1,2,7–9] We have made use of these properties and have been successful in using it to control dimensionality. The choice of solvent is also a determining factor. Thus a variety of chain or sheet structures have been obtained as well as the

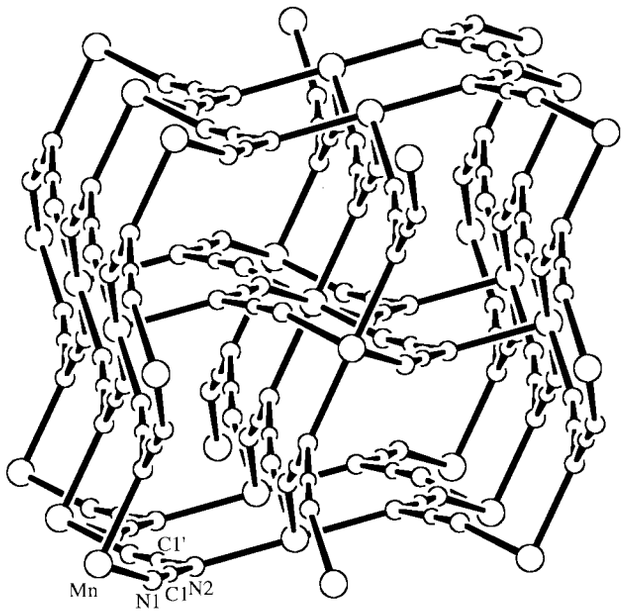

Fig. 1 Rutile-like network and atom numbering in α-$Mn(dca)_2$.

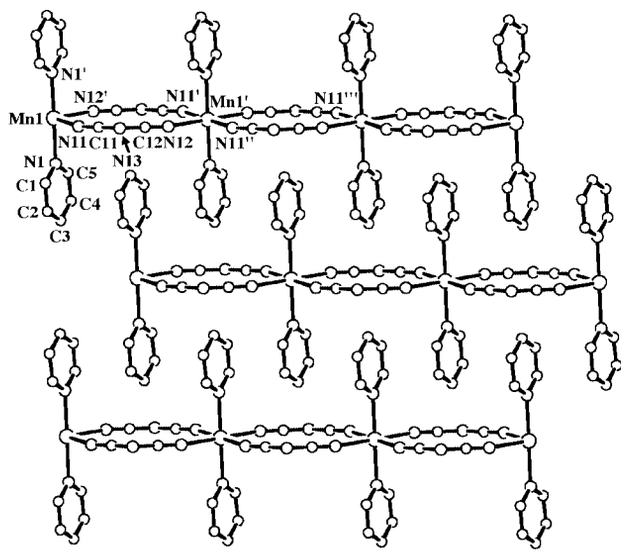

Fig. 2 The atom numbering scheme and interdigitating chains in the structure of $[Mn(dca)_2(py)_2]$.

parent rutile-like network. In separate work,[8] the use of 'linker' ligands such as pyrazine and 4,4′-bipyridine to bridge $\{M(dca)_2\}_n$ chains and sheets has generated 2-D and 3-D structures, a number of which interpenetrate.

α-$Mn(dca)_2$. The crystal structure of α-$Mn(dca)_2$ is composed of a polymeric network containing only four crystallographically unique atoms (Mn, N1, C1 and N2). Each Mn cation is co-ordinated to six dca ligands, and each dca ligand is co-ordinated to three cations, through both the nitrile nitrogens (Mn–N1 2.189(1) Å) and the amido nitrogens (Mn–N2 2.290(2) Å). The topology of the co-ordination network formed is that of rutile, with 6-connecting centres (metal atoms) and 3-connecting centres (dca ligands) in the ratio of 1:2 (Fig. 1). Selected bond lengths and angles are given in Table 2.

The structure is isomorphous with the related compounds α-$M(dca)_2$, M = Co, Ni or Cu.[1,2,7] The volume of the orthorhombic unit cell of α-$Mn(dca)_2$ is the largest of the series, reflecting its larger ionic radius. While the structure of α-$Cu(dca)_2$ shows appreciable Jahn–Teller distortion, the metal–nitrogen distances in α-$Mn(dca)_2$ are comparable and are longer than those seen in α-$Co(dca)_2$. As with α-$Cu(dca)_2$ and α-$Co(dca)_2$,[1,2,7] there are considerable distortions in the

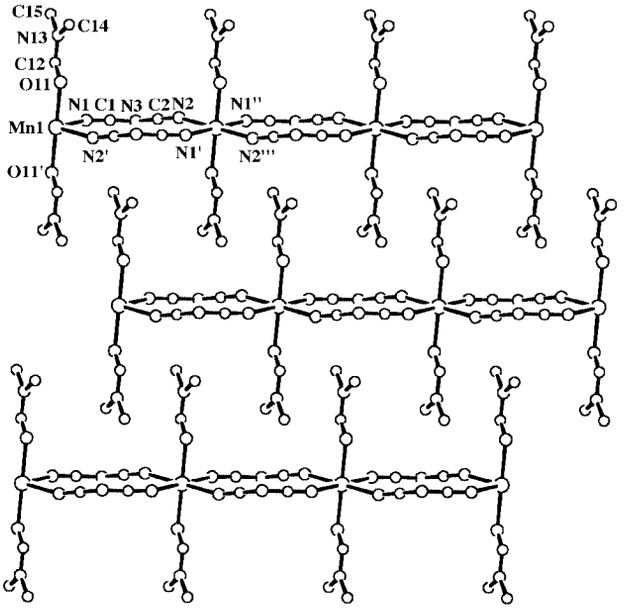

Fig. 3 The atom numbering scheme and interdigitating chains in the structure of $[Mn(dca)_2(DMF)_2]$.

α-$Mn(dca)_2$ network, possibly due to π–π interactions between pairs of dca ligands across the square channels (closest contacts being C1 · · · C1 3.493, N2 · · · N2 3.670 Å).

$[Mn(dca)_2(py)_2]$. The structure of $[Mn(dca)_2(py)_2]$ consists of linear chains (Fig. 2, Table 3). Each Mn atom lies on an inversion centre, and is connected to two others by four equatorially bound dca ligands participating in two $Mn(dca)_2Mn$ bridges (Mn(1)–N(11) = 2.222(3), Mn(1)–N(12) 2.220(3) Å). The dca ligands are two-connecting, with only the nitrile nitrogens involved in bonding interactions with the metal atoms. Interestingly, the $M_2(dca)_2$ rings in this structure, and indeed in all the structures reported here containing such rings, have a slight chair conformation. The octahedral co-ordination environments of the cations are completed by co-ordination of two *trans* pyridine ligands (Mn(1)–N(1) 2.260(3) Å). The chains propagate parallel to the *a* axis, with the Mn · · · Mn distance along the chain being equal to the *a* cell length, 7.5212(3) Å. Similar chains also appear in the rutile-like α-$Mn(dca)_2$, although in this case the axial sites of the manganese are occupied by the amide nitrogen atoms of the dicyanamide ligands in adjacent chains rather than co-ordinated pyridine ligands.

The chains are extensively interdigitated, with the pyridine ligands of adjacent chains overlapping to provide stacks. The distances between the pyridine rings in the stacks are dictated by the repeat distance of the chains, and the 3.543 and 3.601 Å distances between the mean planes are indicative of weak π-stacking interactions.

$[Mn(dca)_2(DMF)_2]$. The structure of $[Mn(dca)_2(DMF)_2]$ contains interdigitated linear chains analogous to those in the pyridine adduct. The Mn atoms again lie on inversion centres (Fig. 3, Table 4) and are co-ordinated to four equatorial dca ligands (Mn(1)–N(1) 2.218(2), Mn(1)–N(2) 2.203(2) Å) and two axial solvent molecules (Mn(1)–O(11) 2.199(2) Å). The chains propagate parallel to the *b* axis, with the intrachain Mn · · · Mn distance (the *b* axis length, 7.4907(4) Å) slightly shorter than for the pyridine adduct. The chains interdigitate such that each DMF ligand lies between two DMF ligands of an adjacent chain, with the mean planes of the non-hydrogen atoms being 3.369 and 3.542 Å apart.

$[M(dca)_2(CH_3OH)_2]$, M = Mn or Fe. The structure of $[Mn(dca)_2(CH_3OH)_2]$ also contains linear chains. The Mn atoms lie on sites of 2/*m* symmetry (Fig. 4, Table 5) and co-ordinate to four dca ligands (Mn(1)–N(1) 2.212(1) Å) and two *trans* sol-

Table 1 Crystallographic data

	$Mn(dca)_2$	$[Mn(dca)_2(py)_2]$	$[Mn(dca)_2(DMF)_2]$	$[Mn(dca)_2(CH_3OH)_2]$	$[Fe(dca)_2(CH_3OH)_2]$	$[Mn(dca)_2(C_2H_5OH)_2]$	$[Mn(dca)_2(H_2O)_2]\cdot H_2O$
Formula	C_4MnN_6	$C_{14}H_{10}MnN_8$	$C_{10}H_{14}MnN_8O_2$	$C_6H_8MnN_6O_2$	$C_6H_8FeN_6O_2$	$C_{11}H_{18}MnN_6O_3$	$C_4H_6MnN_6O_3$
M	187.04	345.24	333.23	251.12	252.03	337.25	241.09
Crystal system	Orthorhombic	Monoclinic	Triclinic	Monoclinic	Monoclinic	Monoclinic	Monoclinic
Space group	*Pnnm*	$P2_1/n$	$P\bar{1}$	$C2/m$	$C2/m$	$C2/c$	$P2_1/n$
a/Å	7.2723(3)	7.5212(3)	6.4242(3)	12.409(1)	12.2247(7)	11.316(1)	7.3165(2)
b/Å	6.1126(3)	13.1458(9)	7.4907(4)	7.481(1)	7.3921(5)	11.358(1)	11.6229(5)
c/Å	7.5563(4)	8.6087(6)	8.4034(4)	6.528(1)	6.4610(4)	12.488(1)	11.3590(5)
α/°			103.021(3)				
β/°		115.183(9)	106.485(4)	119.979(3)	120.119(1)	96.918(3)	103.241(5)
γ/°			99.390(4)				
U/Å^3	335.90(3)	770.26(8)	366.46(3)	524.93(11)	505.03(5)	1593.4(2)	940.28(6)
Z	2	2	1	2	2	4	4
T/K	123(2)	123(2)	123(2)	150(2)	123(2)	150(2)	123(2)
μ(Mo-Kα)/mm^{-1}	1.896	0.868	0.918	1.248	1.484	0.847	1.397
Data collected	1155	2803	3174	1764	3366	5757	3453
Unique data (R_{int})	413 (0.026)	1612 (0.1137)	1460 (0.023)	538 (0.022)	664 (0.057)	1567 (0.026)	1787 (0.031)
Observed reflections [$I > 2\sigma(I)$]	376	1002	1316	537	584	1562	1417
Parameters	29	106	97	51	51	142	154
Final $R1$, $wR2$ [$I > 2\sigma(I)$]	0.0249, 0.0629	0.0509, 0.1053	0.0415, 0.1268	0.0237, 0.0577	0.0424, 0.0874	0.0433, 0.0854	0.0313, 0.0926
(all data)	0.0287, 0.0645	0.1034, 0.1200	0.0464, 0.1289	0.0238, 0.0578	0.0555, 0.0926	0.0437, 0.0855	0.0440, 0.0992
Goodness of fit, S	1.133	1.067	1.234	1.257	1.089	1.445	1.175

Table 2 Selected bond distances (Å) and angles (°) for α-$Mn(dca)_2$

Mn–N(1)	2.189(1)	Mn–N(2)	2.290(2)
N(1)–C(1)	1.152(2)	C(1)–N(2^i)	1.319(2)
N(1)–Mn–N(1^{ii})	85.33(7)	N(1)–Mn–N(2)	90.93(5)
Mn–N(1)–C(1)	158.9(1)	Mn–N(2)–C(1^{iii})	119.76(9)
C(1^{iii})–N(2)–C(1^{iv})	118.1(2)	N(1)–C(1)–N(2^i)	174.9(2)

Symmetry transformations: (i) $x - \frac{1}{2}, \frac{1}{2} - y, z + \frac{1}{2}$; (ii) $-x, -y, z$; (iii) $x + \frac{1}{2}, \frac{1}{2} - y, z - \frac{1}{2}$; (iv) $x + \frac{1}{2}, \frac{1}{2} - y, \frac{1}{2} - z$.

Table 3 Selected bond distances (Å) and angles (°) for $[Mn(dca)_2(py)_2]$

Mn(1)–N(11)	2.222(3)	Mn(1)–N(12^i)	2.220(3)
Mn(1)–N(1)	2.260(3)	N(11)–C(11)	1.156(4)
C(11)–N(13)	1.303(4)	N(12)–C(12)	1.157(4)
C(12)–N(13)	1.297(4)		
N(1)–Mn(1)–N(11)	90.0(1)	N(1)–Mn(1)–N(12^i)	89.5(1)
N(11)–Mn(1)–N(12^i)	89.1(1)	Mn(1)–N(11)–C(11)	154.7(3)
Mn(1^{ii})–N(12)–C(12)	163.4(3)	C(11)–N(13)–C(12)	119.9(3)
N(13)–C(11)–N(11)	174.2(4)	N(13)–C(12)–N(12)	174.0(4)

Symmetry transformations: (i) $1 - x, -y, 1 - z$; (ii) $x + 1, y, z$.

Table 4 Selected bond distances (Å) and angles (°) for $[Mn(dca)_2(DMF)_2]$

Mn(1)–N(1)	2.218(2)	Mn(1)–N(2^i)	2.203(2)
Mn(1)–O(11)	2.199(2)	N(1)–C(1)	1.156(3)
C(1)–N(3)	1.303(4)	C(2)–N(3)	1.302(3)
N(2)–C(2)	1.155(3)	O(11)–C(12)	1.248(3)
C(12)–N(13)	1.316(3)	N(13)–C(14)	1.459(3)
N(13)–C(15)	1.455(3)		
N(1)–Mn(1)–O(11)	89.14(7)	N(1)–Mn(1)–N(2^i)	91.64(8)
Mn(1)–N(1)–C(1)	144.8(2)	Mn(1^{ii})–N(2)–C(1)	162.7(2)
N(1)–C(1)–N(3)	173.5(3)	N(2)–C(2)–N(3)	173.5(3)
C(1)–N(3)–C(2)	120.6(2)	Mn(1)–O(11)–C(12)	121.4(2)
O(11)–C(12)–N(13)	124.7(2)	C(12)–N(13)–C(14)	122.0(2)
C(12)–N(13)–C(15)	120.9(2)	C(14)–N(13)–C(15)	117.1(2)

Symmetry transformations: (i) $x, y + 1, z$; (ii) $x, y - 1, z$.

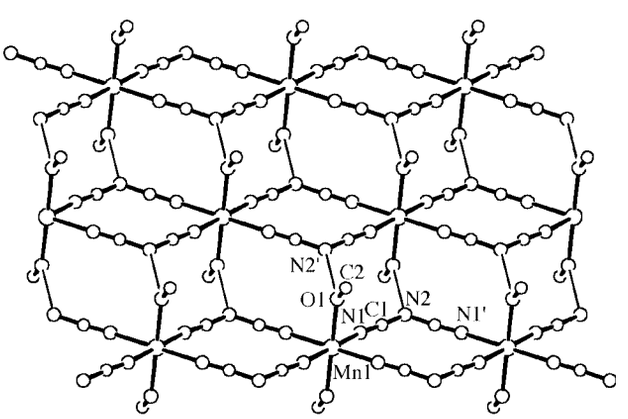

Fig. 4 The atom numbering scheme and chain-like structure $[Mn(dca)_2(CH_3OH)_2]$. The thin lines represent hydrogen bonding interactions between adjacent chains (hydrogen atoms not shown for clarity). The structure of $[Fe(dca)_2(CH_3OH)_2]$ is isomorphous.

vent molecules (Mn(1)–O(1) 2.172(2) Å). The chain structure is analogous to that found for $[Ni(NCS)_2(NH_3)_2]$.[19] The chains propagate parallel to the *b* axis, with the intrachain Mn ··· Mn distance being equal to the *b* cell length (7.481(1) Å). The chains are cross-linked by hydrogen bonds between the alcohol and dca ligands (*via* the amide nitrogen, O1 ··· N2 2.791(3)Å) of adjoining chains. This results in 2-D layers, as shown in Fig. 4, which project along the $(a + 2c)$ direction. The structure of $[Fe(dca)_2(CH_3OH)_2]$ is isomorphous, and the important bond distances and angles are given in Table 5.

While this manuscript was in preparation, Miller and co-workers[20] also reported the crystal structure of $[Fe(dca)_2(CH_3OH)_2]$ containing an almost identical unit cell with systematic absences consistent with the non-centrosymmetric space groups *Cm* and *C*2, and a satisfactory solution could only be obtained in *C*2. They did not, however, report investigating the centrosymmetric space group *C*2/*m*, which has the same systematic absences as *Cm* and *C*2. When we re-examined our structure in *C*2 we found that there were high correlations between chemically equivalent atoms which become crystallographically equivalent in *C*2/*m*. Our *C*2 solution also contained one non-positive-definite atom, generated a Flack parameter of *ca*. 0.5, and gave higher *R* values. All these results point to the centrosymmetric solution being correct. Close inspection of the co-ordinates of the Miller solution indicate that, upon translating the structure by $\Delta x = -0.5$ and $\Delta y = -0.133$ (such that Fe resides on the origin), the co-ordinates of the chemically equivalent pairs N1/N3 and C2/C3 are very close to x,y,z and $x,-y,z$, indicating the presence of a mirror plane (Fe, O1, N2 and C1 all lie on this mirror plane). The largest deviation of the co-ordinates required to impose this mirror plane (and generate our solution) is 0.075 Å. Thus we feel *C*2/*m* is a more appropriate space group.[21]

Table 5 Selected bond distances (Å) and angles (°) for $[M(dca)_2(CH_3OH)_2]$, M = Mn or Fe

	Mn	Fe
M(1)–N(1)	2.212(2)	2.150(2)
M(1)–O(1)	2.172(2)	2.088(3)
N(1)–C(1)	1.152(2)	1.149(3)
C(1)–N(2)	1.312(2)	1.317(3)
O(1)–C(2)	1.418(3)	1.426(5)
N(1)–M(1)–O(1)	90.34(5)	89.96(8)
N(1)–M(1)–N(1^i)	88.57(7)	87.65(11)
C(1)–N(1)–M(1)	160.3(1)	161.1(2)
N(1)–C(1)–N(2)	175.4(2)	175.7(3)
C(1)–N(2)–C(1^{ii})	118.0(2)	117.0(3)
C(2)–O(1)–M(1)	131.4(2)	131.2(3)

Symmetry transformations: (i) $-x, y, -z$; (ii) $x, 1 - y, z$.

$[Mn(dca)_2(C_2H_5OH)_2]\cdot(CH_3)_2CO$. The metal and ligand co-ordination environments in $[Mn(dca)_2(C_2H_5OH)_2]\cdot(CH_3)_2CO$ are similar to those of the methanolate (Table 6). The metal is co-ordinated to four equatorial dca ligands and two axial alcohol ligands, while the dca ligands again co-ordinate to two metals *via* the nitrile nitrogens only. In this structure, however, the resultant topology is that of a pseudo square-grid sheet, with each Mn atom connected to *four* neighbouring metals *via* the bridging dca ligands (Fig. 5). A similar (4,4) sheet structure is found for $[Mn(SCN)_2(C_2H_5OH)_2]$.[22] Close examination of the difference maps revealed a small amount of disorder in the ethyl part of the ethanol molecule; this refined well as the sum of two different conformations, the major fragment being refined anisotropically with fixed 90% occupation and the minor fragment being refined isotropically with fixed 10% occupation. The alcohol ligands again participate in hydrogen bonding interactions (O1 ··· O11 2.789(2)Å), this time with guest acetone molecules included between the sheets. Each acetone molecule participates in two equivalent interactions to adjoining layers (Fig. 6).

$[Mn(dca)_2(H_2O)_2]\cdot H_2O$. The structure of $[Mn(dca)_2(H_2O)_2]\cdot H_2O$ combines both the chain and sheet topologies seen above. Sheets of composition $Mn(dca)_2(H_2O)_2$ stack in a fashion that results in square channels running through the structure. These spacious channels are occupied by polymeric linear chains which have an identical chemical composition to the sheets (Fig. 7(a)).

Within both the sheets and the chains all Mn atoms, all H_2O

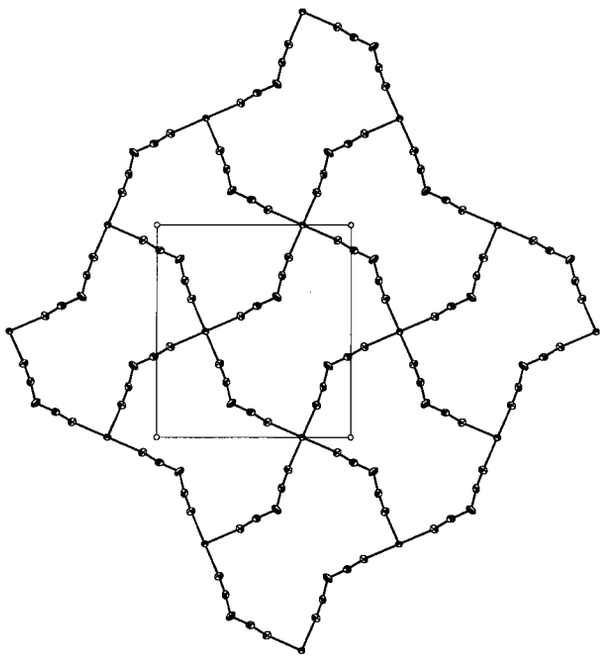

Fig. 5 The $Mn(dca)_2$ sheet-like structure in $[Mn(dca)_2(C_2H_5OH)_2]\cdot(CH_3)_2CO$, with solvent molecules omitted for clarity.

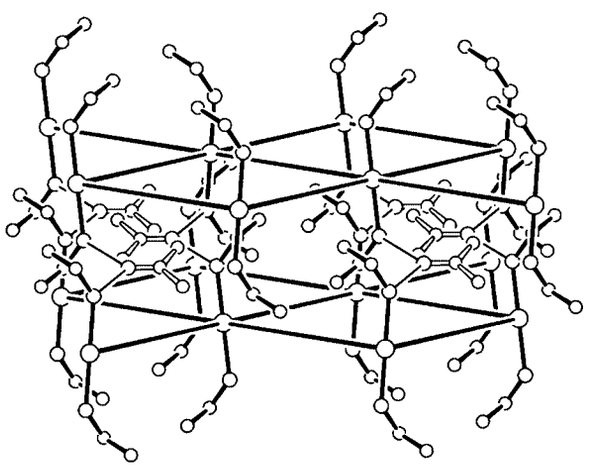

Fig. 6 The hydrogen bonding interactions (thin lines) between co-ordinated ethanol ligands (solid lines) and intercalated acetone molecules (open lines) in $[Mn(dca)_2(C_2H_5OH)_2]\cdot(CH_3)_2CO$. For clarity, the dca ligands bridging the metal atoms are represented simply as solid lines, and hydrogen atoms are omitted.

ligands and all dca ligands are equivalent. Both the sheet Mn atoms and the chain Mn atoms are co-ordinated to four equatorial, two-connecting dca ligands and two terminal axial water ligands. In the sheets the Mn atoms are connected to four neighbours by four Mn(dca)Mn bridges, whilst in the chains each Mn atom is connected to two others by two $Mn(dca)_2Mn$ bridges. The metal donor atom bond lengths for the two types of metal atoms are very similar (Table 7).

The structure also contains clathrated water molecules (O3), which participate in polymeric hydrogen bonded networks (Fig. 7(b)). These complicated networks (all of which are equivalent) have a sheet topology, and are found between any pairs of adjacent $Mn(dca)_2(H_2O)_2$ sheets. They involve the water molecules and dca ligands (*via* the unco-ordinated amido nitrogens) belonging to both the chains and the sheets, and the intercalated water. Each clathrated water hydrogen bonds to two sheet waters, one chain water, and one chain dca ligand. The sheet waters in turn each hydrogen bond to two clathrate waters and one chain water, while each of the chain waters interacts with one sheet water, one clathrate water and one sheet dca ligand.

Table 6 Selected bond distances (Å) and angles (°) for $[Mn(dca)_2(C_2H_5OH)_2]\cdot(CH_3)_2CO$

Mn(1)–N(1)	2.189(2)	Mn(1)–N(3^{i})	2.233(2)
Mn(1)–O(1)	2.200(2)	C(1)–N(1)	1.148(3)
N(2)–C(1)	1.300(3)	N(2)–C(2)	1.300(3)
C(2)–N(3)	1.147(3)	O(1)–C(3)	1.437(3)
C(3)–C(4)	1.506(4)	O(11)–C(11)	1.224(4)
C(11)–C(12)	1.487(3)		
N(1)–Mn(1)–N(3^{i})	89.16(8)	N(1)–Mn(1)–O(1)	92.14(8)
O(1)–Mn(1)–N(3^{i})	90.70(8)	C(1)–N(1)–Mn(1)	167.9(2)
N(2)–C(1)–N(1)	172.8(3)	C(1)–N(2)–C(2)	123.4(2)
N(2)–C(2)–N(3)	172.8(3)	C(2)–N(3)–Mn(1^{ii})	164.6(2)
Mn(1)–O(1)–C(3)	130.7(2)	O(1)–C(3)–C(4)	112.3(3)
O(11)–C(11)–C(12)	121.1(2)	C(12)–C(11)–C(12^{iii})	117.7(3)

Symmetry transformations: (i) $\frac{1}{2} - x, y - 1, \frac{1}{2} - z$; (ii) $\frac{1}{2} - x, y + \frac{1}{2}, \frac{1}{2} - z$; (iii) $-x, y, \frac{1}{2} - z$.

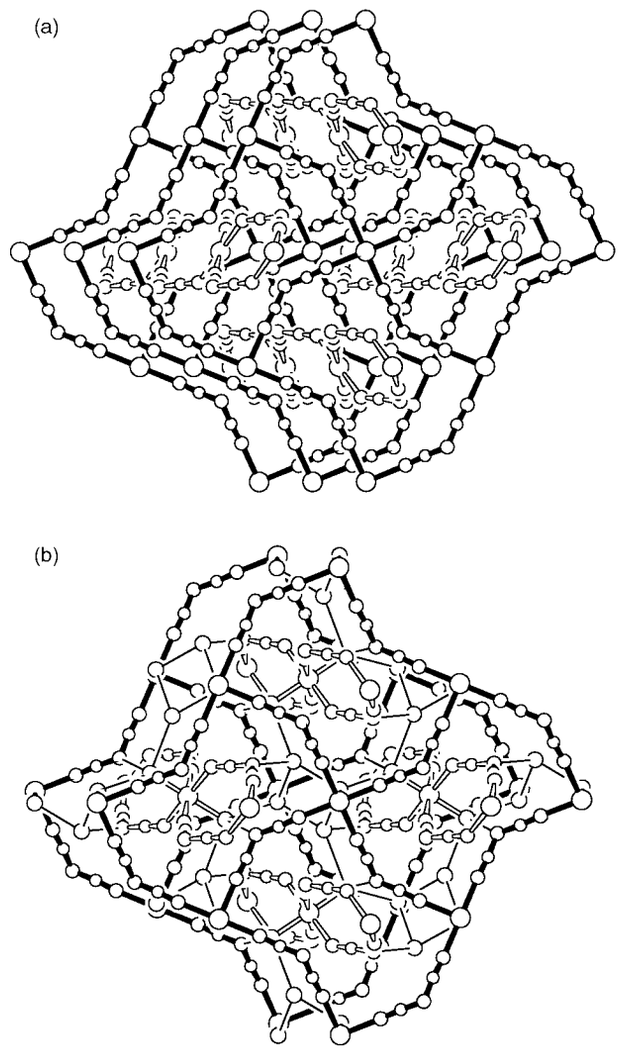

Fig. 7 (a) The intercalation of $Mn(dca)_2$ chains in square channels formed by the stacking of $Mn(dca)_2$ sheets in the structure of $[Mn(dca)_2(H_2O)_2]\cdot H_2O$. The water molecules are omitted for clarity. (b) The hydrogen bonding sheet structure (thin lines) for $[Mn(dca)_2(H_2O)_2]\cdot H_2O$, which involves intercalated water molecules, and dca and water ligands in both the chains and the sheets. Circles represent, in order of increasing size, C, N, O and Mn, and hydrogen atoms are omitted for clarity.

Magnetic properties

α-$Mn(dca)_2$. We have recently[12] described preliminary data on this rutile-like phase and give further details here. Samples studied at Monash University and in Strasbourg were prepared independently and generally gave the same results. They were

Table 7 Selected bond distances (Å) and angles (°) for $[Mn(dca)_2(H_2O)_2]\cdot H_2O$

Mn(1)–N(1)	2.202(2)	Mn(1)–N(2^{i})	2.179(2)
Mn(1)–O(1)	2.227(2)	Mn(2)–O(2)	2.223(2)
Mn(2)–N(4)	2.184(2)	Mn(2)–N(5^{ii})	2.201(2)
C(1)–N(1)	1.154(3)	C(2)–N(2)	1.151(3)
N(3)–C(1)	1.313(3)	N(3)–C(2)	1.307(3)
C(4)–N(4)	1.149(3)	C(5)–N(5)	1.161(3)
N(6)–C(4)	1.317(3)	N(6)–C(5)	1.308(3)
N(1)–Mn(1)–O(1)	92.76(7)	N(2^{i})–Mn(1)–O(1)	87.74(7)
N(1)–Mn(1)–N(2^{i})	89.92(7)	N(4)–Mn(2)–N(5^{ii})	89.65(8)
N(4)–Mn(2)–O(2)	94.68(7)	N(5^{ii})–Mn(2)–O(2)	90.13(7)
C(1)–N(1)–Mn(1)	170.5(2)	C(2)–N(2)–Mn(1^{iii})	173.0(2)
C(4)–N(4)–Mn(2)	161.6(2)	C(5)–N(5)–Mn(2^{iv})	139.6(2)
N(1)–C(1)–N(3)	174.8(2)	N(2)–C(2)–N(3)	173.9(2)
C(1)–N(3)–C(2)	119.2(2)	C(4)–N(6)–C(5)	117.3(2)
N(4)–C(4)–N(6)	175.4(2)	N(5)–C(5)–N(6)	175.3(2)

Symmetry transformations: (i) $-x-\frac{1}{2}, y+\frac{1}{2}, \frac{3}{2}-z$; (ii) $x+1, y, z$; (iii) $-x-\frac{1}{2}, y-\frac{1}{2}, \frac{3}{2}-z$; (iv) $x-1, y, z$.

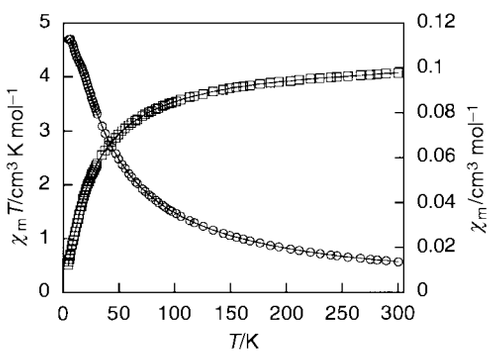

Fig. 8 Temperature dependence of χ_m (○) and the product $\chi_m T$ (□) for α-$Mn(dca)_2$ (Monash sample). $H = 10\,000$ Oe. The solid lines are guides to the eye.

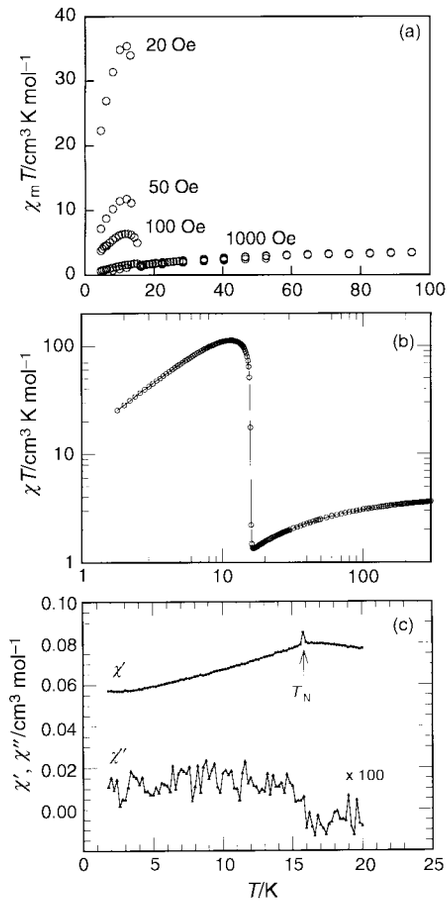

Fig. 9 Temperature dependence of the product $\chi_m T$ for (a) Monash sample of α-$Mn(dca)_2$ at the low field values shown, (b) Strasbourg sample B of α-$Mn(dca)_2$, $H = 3$ Oe, (c) AC susceptibility for Strasbourg sample B in a field of 1 Oe oscillating at 20 Hz.

analytically pure and their powder XRD patterns showed good agreement to that predicted from the crystal structure. One crystalline sample was used at Monash for all measurements. Two samples were used at Strasbourg, sample A being a powder, B being crystalline. The latter was used for all measurements except that of heat capacity. In a DC field of 1T the χT value at 300 K of 4.073 cm^3 K mol^{-1} decreases gradually by a small amount as the temperature is decreased to *ca.* 50 K, then a little more steeply, reaching 0.507 cm^3 K mol^{-1} at 4.5 K (Fig. 8). Such behaviour is indicative of weak antiferromagnetic coupling occurring, influenced to a small degree by zero-field splitting of the $^6A_{1g}$ single-ion states. The corresponding χ *vs.* T curve is Curie-Weiss like in shape, with an inflection occurring at *ca.* 16 K and a levelling off in χ below *ca.* 6 K. The Weiss and Curie constants in the range 20–300 K under a 1 T field are $\theta = -25$ K and C = 4.42 cm^3 K mol^{-1}. The same behaviour occurs in a 0.5 T field, but, as is evident in Fig. 9(a), an abrupt break in χT occurs at 16 K when lower fields are employed. In a 20 Oe field, for instance, χT rises abruptly towards a maximum of 35.46 cm^3 K mol^{-1} at 12 K (16.84 μ_B) prior to decreasing rapidly as the temperature approaches 4.2 K. The minimum value of χT prior to the abrupt increase is 1.338 cm^3 K mol^{-1} (3.27 μ_B). This transition at 16 K is indicative of the onset of long-range magnetic ordering. The same behaviour was observed at Strasbourg on sample B in a field of 3 Oe, with χT reaching a maximum of 115.2 cm^3 K mol^{-1} at 12 K, Fig. 9(b). A sharp peak at $T_N = 16$ K was observed in the AC in-phase susceptibility plot of χ' *vs.* temperature in a field of $H_{AC} = 1$ Oe (Fig. 9(c)). The existence of an out-of-phase inflection at 16 K in the χ'' plot, though very weak, confirms long-range ordering is present.

Further to confirm the occurrence of a magnetic phase transition, the DC magnetisation was measured with the sample cooled in zero-field (ZFCM) and in a field of 5 Oe (FCM). It can be seen in Fig. 10(a) that the FCM shows a rapid increase below 16 K and continues to increase more gradually while the temperature is lowered to 4.5 K, with an upward discontinuity at 6.5 K. The latter feature may be intrinsic to α-$Mn(dca)_2$ since it also appears in the heat capacity data (see below) and in the magnetisation data measured on a desolvated sample[2] of $[Mn(dca)_2(C_2H_5OH)]\cdot(CH_3)_2CO$ both made and measured in Strasbourg. However, as seen in Fig. 10(b), it did not appear in the 0.1 Oe FCM plot of sample B in Strasbourg measured down to 1.8 K, which was otherwise identical to Fig. 10(a). Further studies are in progress on the 6 K feature.‡

The remnant magnetisation (RM; Fig. 10(a)) follows the FCM curve. The ZFCM values are very small in size, and constant, below T_N. The complex α-$Mn(dca)_2$ displays hysteresis in its magnetisation. The *M vs. H* loops were measured at Monash University on a loose powder, at 5 K (Fig. 11(a)), and on a Vaseline dispersed mull at 2 K (similar to inset of Fig. 11(b)), the latter procedure followed in order to eliminate any torquing of crystallites, a feature which is particularly marked in α-$Fe(dca)_2$,[2,11] but less so in α-$Mn(dca)_2$. The differences noted in the remnant magnetisation (*viz.* 63 cm^3 mol^{-1} Oe at 5 K for a neat powder and 29 cm^3 mol^{-1} Oe at 2 K for a Vaseline mull) and the coercive field (*viz.* 263 Oe at 5 K for a neat powder and 406 Oe at 2 K for a Vaseline mull) probably reflect temperature and particle size and shape differences rather than torquing

‡ The species responsible for the 6 K feature in now known to be $Mn(dca)_2(H_2O)$, which is present in trace quantities in the samples mentioned. It is also a spin-canted antiferromagnet with a polymeric 3-D structure (S. R. Batten, P. Jensen, B. Moubaraki, K. S. Murray and D. J. Price, unpublished work).

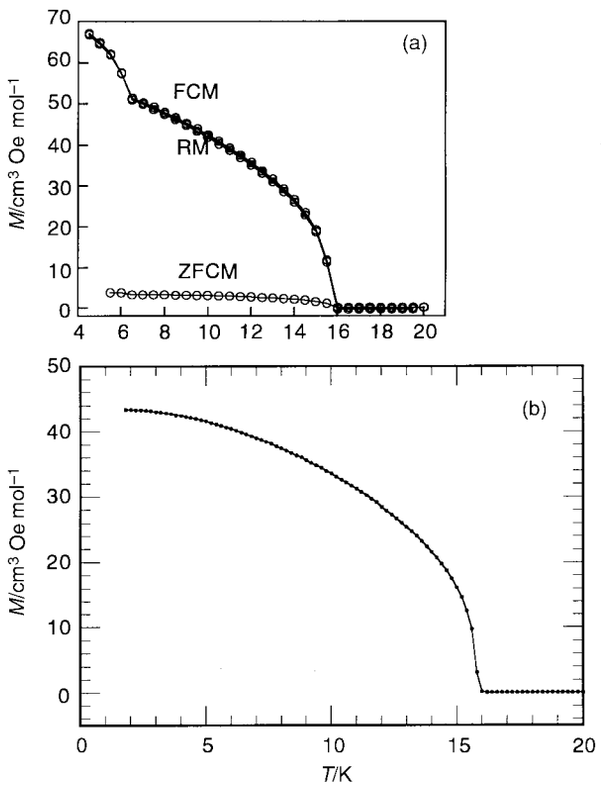

Fig. 10 Temperature dependence of (a) magnetisation, M, of the Monash sample of α-Mn(dca)$_2$ cooled in zero-field (ZFCM) and in field of 5 G (FCM) (remnant magnetisation (RM) is also shown); (b) magnetisation of Strasbourg sample B in an applied field of 0.1 G (FCM).

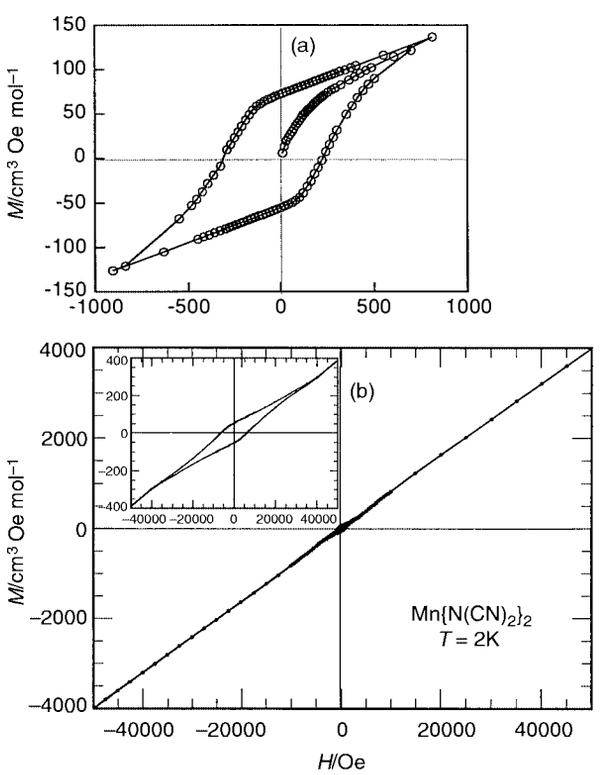

Fig. 11 (a) Hysteresis loops for Monash sample of α-Mn(dca)$_2$ measured as a loose powder up to ±0.1 T at 5 K. (b) Hysteresis loop for Strasbourg sample B measured as a compact powder up to ±5 T at 2 K. The inset shows M values for H varying between ±0.5 T.

effects. A similar dependence of coercive field on particle size has recently been noted by Kahn and co-workers[23] in studies on the hard molecule-based magnet [(Etrad)$_2$Co$_2${Cu(opba)}$_3$]·S

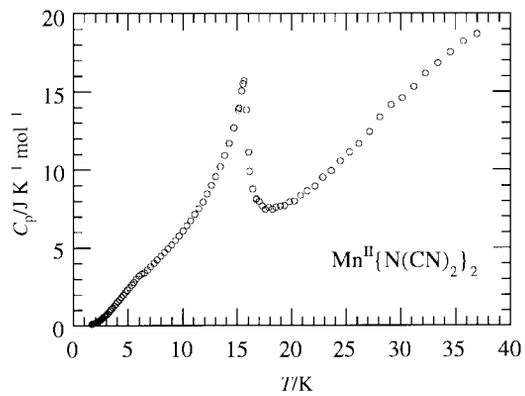

Fig. 12 Temperature dependence of the specific heat of a Strasbourg sample A of α-Mn(dca)$_2$.

where Etrad$^+$ = radical cation, opba = *o*-phenylenebis(oxamate) and S = $DMSO_{1.5}H_2O_{0.25}$.

Temperature dependent hysteresis loops were also measured in Strasbourg using a vibrating sample magnetometer on a powdered sample of B, held tightly in a Delrin container, such that movement of crystallites was not possible. The 4.2 K loop is very similar in shape to that shown in Fig. 11(b). The value of RM (32 cm^3 Oe mol^{-1}) is very similar, but the coercive field is somewhat larger at 625 Oe due, again, to particle size effects.[2,11] The latter value was also obtained on this sample using a SQUID instrument at 2 K, the RM value being a bit larger, 53 cm^3 Oe mol^{-1} (Fig. 11(b)).

High field magnetisation data were measured on a loose powder sample in fields of 0.1 to 5 T, at temperatures between 4.5 and 20 K. The magnetisation increases linearly with field since the moments are being turned against the antiferromagnetic coupling (see also Fig. 11(b)). A value of M of only 0.88 $N\mu_B$ is observed at 4.5 K and 5 T (M_{sat} is expected to be 5 $N\mu_B$). Similar M *vs.* H behaviour was observed for α-Fe(dca)$_2$[2,11] but it contrasts with those observed for the ferromagnets α-Co(dca)$_2$ and α-Ni(dca)$_2$ which show rapid increases in M at low fields and saturation behaviour at high fields.[1,2,7]

Further confirmation of long-range order in α-Mn(dca)$_2$ was provided by heat capacity measurements. The temperature dependence of the total specific heat, C_p, is shown for Strasbourg sample A in Fig. 12. A shoulder is given at 5.95 K and a peak maximum at 15.6 K. The magnetic transition temperature is estimated to be 16 ± 0.2 K in good agreement with the magnetisation results. The estimated magnetic entropy is 3.1 J K^{-1} mol^{-1} when summing to the first shoulder, and 10.1 J K^{-1} mol^{-1} when summing up to 20 K. The $R\ln(2S+1)$ value for $S = 5/2$, appropriate to high-spin Mn^{II}, is 14.9 J K^{-1} mol^{-1}, which is higher than observed. Similar discrepancies were noted in the α-M(dca)$_2$ compounds containing M = Ni, Co or Fe.[2]

In summary, the various magnetic data for α-Mn(dca)$_2$ are consistent with an antiferromagnetically coupled 3-D array of high-spin manganese(II) ions with long-range ordering of the moments occurring below $T_N = 16$ K, to yield a spin-canted antiferromagnetic (weak ferromagnetic) state. An estimated canting angle of 0.05° was obtained from $\sin^{-1}(\mu_{RM}/\mu_{sat})$ where $\mu_{sat} = 5\ \mu_B$ and $\mu_{RM} = 5.2 \times 10^{-3}\ \mu_B$ (from RM = 29 cm^3 Oe mol^{-1}). If RM of 63 cm^3 mol^{-1} Oe is used the canting angle is 0.13°. The small angle for α-Mn(dca)$_2$ compared to that of *ca.* 7.2° for α-Fe(dca)$_2$[2] is consistent with the Dzyaloshinsky–Moriya mechanism,[24] within which the canting angle is proportional to spin–orbit coupling, the ligand field splitting and consequently the deviation of the g value from the free electron value (2.0023). The measured g value is 2.0028. The canting angles in other recently discovered manganese(II) alkylphosphonate magnets vary between 0.1 to 2.9° depending on the alkyl chain length.[25] Further structural relationships of the

Table 8 Summary of magnetic data for α-$Mn(dca)_2$

μ_{eff} (300 K)/μ_B	5.71 ± 0.02 (H = 1 T)[a]
θ/K (25–300 K)	−25 ± 0.5 (H = 1 T)[a]
C/cm^3 K mol^{-1}	4.42 ± 0.02 (H = 1 T)[a]
Coercive field/Oe (2 K)	406 ± 5;[a] 625 ± 5[b]
Remnant magnetisation/cm^3 Oe mol^{-1} (2 K)	29 ± 2;[a] 53 ± 2[b]
M/cm^3 Oe mol^{-1} (4.5 K, 5 T)	4919[a]
T_N/K	16 ± 0.2[a,b]
Maximum in C_p/K	5.95(sh), 15.6
Magnetic entropy/J K^{-1} mol^{-1}	10.1
Canting angle/°	0.05[c]
J/k mean field/K	−0.45

[a] Obtained at Monash University using a SQUID instrument. [b] Obtained at Strasbourg using a SQUID instrument; the RM value was 32 ± 2 cm^3 Oe mol^{-1} at 4.2 K when using a vibrating sample magnetometer. [c] Calculated using RM = 29 cm^3 mol^{-1} Oe and μ_{sat} = 5 μ_B (see text).

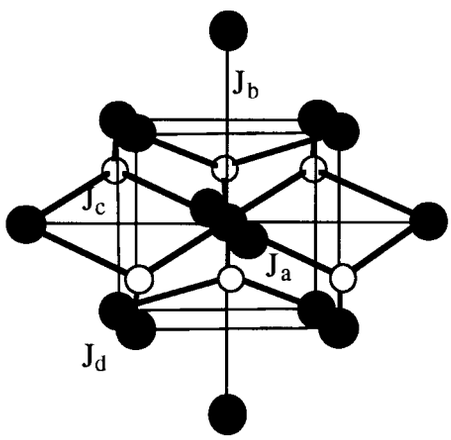

Fig. 13 Definition of the four exchange pathways within the rutile structure of α-$M^{II}(dca)_2$ (only the metals and amide nitrogen are shown for clarity); see ref. 27.

canting angle in α-$Mn(dca)_2$ will require neutron diffraction studies. The magnetic properties are summarised in Table 8. These can be compared to those for the magnets α-$Fe(dca)_2$, α-$Co(dca)_2$ and α-$Ni(dca)_2$[1,2,7] and the spin-canted antiferromagnet β-$Co(dca)_2$ the latter having a 2-D-layered structure containing tetrahedral cobalt(II) ions bridged by 2-connecting dca ligands.[7,26]

The origin of antiferromagnetic coupling in α-$Mn(dca)_2$, of ferromagnetic coupling in the isostructural cobalt(II) and nickel(II) analogues and of paramagnetism in $Cu(dca)_2$ presumably must relate to the net contribution towards J that derives from super exchange pathways involving equatorial Mn–N≡C–N–C≡N–Mn bridges and axial Mn–N≡C–N–Mn bridges. These superexchange ideas had been quantified many years ago by Goodenough.[27] For compounds having the rutile structure he proposed a phase diagram which consists of four possible ground states depending on the ratio of exchange interactions, nowadays called spin frustration (Fig. 13). In the present rutile type structure[2] there are four independent nearest-neighbour magnetic exchange interactions: eight equivalent superexchange (J_d, d for diagonal) *via* M(1)–N(1)–C(1)–N(2)···M(1′) (M···M′ 6.07 Å); two equivalent direct (J_a) along a at 7.27 Å, two (J_b) along b at 6.11 Å and a further two which are a combination of direct and superexchange (J_c) along c at 7.56 Å. Within this structure type the magnetic ground state and Curie temperature, and therefore the size and sign of the exchange interactions, are found to depend greatly on the M–N distances and on the extent of structural distortion. Octahedral manganese(II) centres ($t_{2g}^3e_g^2$) can employ t_{2g} and/or e_g ground state 'magnetic' orbitals as also can Co^{II} ($t_{2g}^5e_g^2$), whilst Ni^{II} ($t_{2g}^6e_g^2$) utilises only e_g orbitals. The axial elongation noted in the crystal

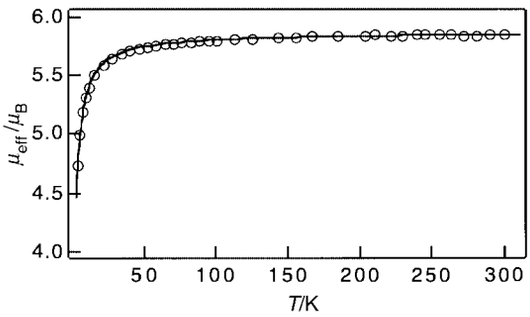

Fig. 14 Temperature dependence of effective magnetic moment, μ_{eff} (=2.828 ($\chi_m T$)$^{1/2}$), for $[Mn(dca)_2(DMF)_2]$. The solid line is the best fit by the linear chain Heisenberg model[28] with g = 2.00, J = −0.12 cm^{-1} (D assumed to be zero).

structures means that both the e_g and t_{2g} orbital energies will be split with z-containing orbitals being lower in energy. From the observed coupling in the α-$M(dca)_2$ series the e_g/e_g and t_{2g}/t_{2g} combinations are expected to be ferromagnetic whilst t_{2g}/e_g antiferromagnetic. This is evident from the series spanning α-$Ni(dca)_2$ (ferromagnetic) to α-$Mn(dca)_2$ (antiferromagnetic) in which removal of electrons from the t_{2g} orbitals leads to additional interactions of type t_{2g}/t_{2g} and t_{2g}/e_g resulting in antiferromagnetic contributions dominating over ferromagnetic contributions, as in the cases of α-$Fe(dca)_2$ and α-$Mn(dca)_2$. One can predict α-$V(dca)_2$, with a t_{2g}^3 configuration, to be weakly ferromagnetic, probably with a lower T_c value than that of α-$Ni(dca)_2$.

Chain and sheet complexes $[Mn(dca)_2(L)_2]$

The magnetic properties of these compounds are all rather similar with Curie–Weiss behaviour observed in the temperature range 4.2–300 K and μ_{eff} values, per Mn^{II}, of *ca.* 5.85 μ_B at 300 K. No long-range order was noted even in those systems such as L = CH_3OH in which the chains are connected *via* hydrogen bonding (see below), or in the layered structures, L = C_2H_5OH and H_2O, although any partial desolvation of the latter two compounds can yield contaminating α-$Mn(dca)_2$ with its characteristic T_c of 16 K in very low fields.[2] A typical set of experimental magnetic moment data in a field of 1 T is given for L = DMF in Fig. 14. The μ_{eff} values remain constant down to *ca.* 40 K then decrease rapidly to 4.72 μ_B at 4.2 K. There are two contributions to such μ_{eff}/T behaviour for a manganese(II), (d^5) system, zero-field splitting and short range antiferromagnetic coupling. The splitting of the single-ion $^6A_{1g}$ state by spin–orbit coupling in zero field is expected to be very small and will be ignored. The short range antiferromagnetic coupling was simulated by use of a 1-D Heisenberg chain model ($-2J\tilde{S}_1\cdot\tilde{S}_2$) developed by Fisher[28] and applied commonly to manganese(II) chain systems.[29] The best-fit values of g and J obtained from eqn. (1) are given in Table 9.

$$\chi = \frac{Ng^2\beta^2S(S+1)}{3kT}\cdot\frac{1+u}{1-u} \qquad (1)$$

$$u = \coth\left[\frac{2JS(S+1)}{kT}\right] - \frac{kT}{2JS(S+1)}$$

The very small values of J indicate that weak antiferromagnetic intrachain interactions are mediated by the $Mn(N{\equiv}C{-}N{-}C{\equiv}N)_2Mn$ pathways. Given that within the rutile structure the chains are similar we can conclude that J_c in the above discussion is of the same order of magnitude, thereby consistent with our proposal that J_d is the dominant driving interaction in observed ground states. Interchain interactions are anticipated to be weaker in the 1-D systems and due to the lack of bonding pathways there can only be dipolar interaction

Table 9 Curie–Weiss data and best fit g and J values for $[Mn(dca)_2(L)_2]$ compounds using the Fisher[28] chain model (L = CH_3OH, DMF, pyridine or H_2O)

	L				
	CH_3OH	C_2H_5OH	DMF	H_2O	py
θ/K	−2.0	−3.0	−2.1	−4.1	−2.4
g	1.98	—[a]	2.00	1.98	1.98
J/cm^{-1}	−0.12	—[a]	−0.12	−0.17	−0.12

[a] Not fitted because of desolvation effects.[2]

between chains at large distance. Earlier work by Hvastijová and co-workers[13] on chain systems of $[M(dca)_2(L)_2]$, M = Co, Ni or Cu, showed similar short range antiferromagnetism. Strictly a 2-D model of the type developed by Rushbrooke and Wood[30] should be used for the sheet systems with $L_2 = (C_2H_5OH)_2$ or $(H_2O)_2$. In fact, since the latter contains both chains and sheets, a combination of the two models may be warranted. However, since the observed magnetic data are relatively featureless and so similar between the chain and sheet structures, it is anticipated that the J values will be the same using 1-D or 2-D models.

We have not been able to obtain sufficient amounts of $[Fe(dca)_2(CH_3OH)_2]$ free of other products when using $Fe(ClO_4)_2 \cdot 6H_2O$ as starting reagent. However, like its manganese(II) analogue, we anticipate weak antiferromagnetic intrachain coupling to occur without any long range order. It is unlikely that the J value will be large enough to detect a Haldane gap with $\Delta S = 2$. In their very recent report on $[Fe(dca)_2(CH_3OH)_2]$ prepared in good yield from $Fe(BF_4)_2 \cdot 6H_2O$, Miller and co-workers[20] observed just such weak antiferromagnetic coupling.

Conclusion

This work has shown the versatility that the dicyanamide bridging ligand can display in its co-ordination to metal ions such as Mn^{II}. Tridentate co-ordination occurs in α-$Mn(dca)_2$ to yield the 3-D rutile like single network. Bidentate (nitrile) co-ordination occurs in the linear chain $[Mn(dca)_2(L)_2]$ adducts and in the sheet systems (L = C_2H_5OH and H_2O). The complex α-$Mn(dca)_2$ provides another example of the growing field of spin-canted molecular antiferromagnets and has a T_N of 16 K with low values of coercive field and remnant magnetisation. This magnetic behaviour is similar to that found in α-$Fe(dca)_2$[2,11] but contrasts with the ferromagnetic order observed in α-$Co(dca)_2$ and α-$Ni(dca)_2$.[1,2,7] A simple orbital correlation model and a superexchange model, first applied by Goodenough[27] to rutile MO_2 systems, have been used to try to rationalise these differences in the coupling mechanism and in the type of magnetic order as M^{II} varies. Detailed theoretical calculations are certainly required on this system. The chain and sheet structures found in the Lewis base adducts $[Mn(dca)_2(L)_2]$ give rise to very weak intrachain antiferromagnetic coupling and, consequently, a lack of long-range order.

Acknowledgements

This work was supported by an ARC large grant (to K.S.M.), an ARC Postdoctoral Fellowship (to S.R.B.), Centre National de la Recherche Scientifique (France) and the EEC (Molecular Magnetism: from Materials towards Devices: ERBFMRXCT 980181). C.J.K. thanks Christ Church (Oxford) for a Junior Research Fellowship. We are grateful to R. Poinsot and A. Derory (Strasbourg) for useful discussions.

References

1 S. R. Batten, P. Jensen, B. Moubaraki, K. S. Murray and R. Robson, *Chem. Commun.*, 1998, 439.
2 M. Kurmoo and C. J. Kepert, *New J. Chem.*, 1998, **22**, 1515; *Mol. Cryst. Liq. Cryst.*, 1999, in the press.
3 O. Kahn, *Adv. Inorg. Chem.*, 1995, **43**, 179.
4 W. R. Entley and G. S. Girolami, *Science*, 1995, **268**, 397.
5 T. Mallah, S. Thiebaut, M. Verdaguer and P. Veillet, *Science*, 1993, **262**, 1554.
6 M. Kurmoo, Th. Jestädt, S. J. Blundell, C. J. Kepert, A. Lappas, K. Prassides, W. Hayes, B. W. Lovett and F. L. Pratt, unpublished work.
7 J. L. Manson, C. R. Kmety, Q.-Z. Huang, J. W. Lynn, G. M. Bendele, S. Pagola, P. W. Stephens, L. M. Liable-Sands, A. L. Rheingold, A. J. Epstein and J. S. Miller, *Chem. Mater.*, 1998, **10**, 2552.
8 P. Jensen, S. R. Batten, G. D. Fallon, D. C. R. Hockless, B. Moubaraki, K. S. Murray and R. Robson, *J. Solid State Chem.*, 1999, **145**, 387.
9 M. Kurmoo, K. Lattaud, S. Vilminot, A. De Cian and C. J. Kepert, unpublished work.
10 F. D. M. Haldane, *Phys. Rev. Lett.*, 1983, **50**, 1153; G. E. Granroth, M. W. Meisel, M. Chaparala, Th. Jolicoeur, B. H. Ward and D. R. Talham, *Phys. Rev. Lett.*, 1996, **77**, 1616.
11 D. J. Price, B. Sc. Honours Thesis, Chemistry Department, Monash University, November 1998.
12 K. S. Murray, S. R. Batten, B. Moubaraki, D. J. Price and R. Robson, *Mol. Cryst. Liq. Cryst.*, 1999, in the press.
13 J. Mroziński, M. Hvastijová and J. Kohout, *Polyhedron*, 1992, **11**, 2867; M. Hvastijová, J. Kohout, J. Mroziński and L. Jäger, *Pol. J. Chem.*, 1995, **69**, 852; M. Hvastijová, *Collect. Czech. Chem. Commun.*, 1994, **59**, 2611; H. Köhler, A. Kolbe and G. Lux, *Z. Anorg. Allg. Chem.*, 1977, **428**, 103.
14 H. Köhler, *Z. Anorg. Allg. Chem.*, 1964, **331**, 237.
15 Z. Otwinowski and W. Minor, *Methods in Enzymol.*, 1996.
16 G. M. Sheldrick, SHELX 97, Program for crystal structure refinement, University of Göttingen, 1997.
17 G. M. Sheldrick, SHELXS-86, Program for crystal structure determination, in *Crystallographic Computing 3*, eds. G. M. Sheldrick, C. Kruger and R. Goddard, Oxford University Press, Oxford, 1985, 175.
18 G. M. Sheldrick, SHELXL 93, Program for the refinement of crystal structures using single crystal diffraction data, University of Göttingen, 1993.
19 E. Dubler, A. Reller and H. R. Oswald, *Z. Kristallogr.*, 1982, **161**, 265.
20 J. L. Manson, A. M. Arif and J. S. Miller, *J. Mater. Chem.*, 1999, **9**, 979.
21 R. E. Marsh, *Acta Crystallogr., Sect. B*, 1995, **51**, 897.
22 G. C. DeFotis, E. D. Remy and C. W. Scherrer, *Phys. Rev. B*, 1990, **41**, 9074; J. N. McElearney, L. L. Balagot, J. A. Muir and R. D. Spence, *Phys. Rev. B*, 1979, **19**, 306.
23 M. G. F. Vaz, L. M. M. Pinheiro, H. O. Stumpf, A. F. C. Alcântara, S. Golhen, L. Ouahab, O. Cador, C. Mathoniere and O. Kahn, *Chem. Eur. J.*, 1999, **5**, 1486.
24 I. Dzyaloshinsky, *J. Phys. Chem. Solids*, 1958, **4**, 241; T. Moriya, *Phys. Rev.*, 1960, **120**, 91.
25 S. G. Carling, P. Day, D. Visser and R. E. Kremer, *J. Solid State Chem.*, 1993, **106**, 111.
26 P. Jensen, S. R. Batten, G. D. Fallon, B. Moubaraki, K. S. Murray and D. J. Price, *Chem. Commun.*, 1999, 177.
27 J. B. Goodenough, *Magnetism and the Chemical Bond*, Wiley, New York, 1963.
28 M. E. Fisher, *Am. J. Phys.*, 1964, **32**, 343.
29 T. Smith and S. A. Friedberg, *Phys. Rev.*, 1968, **176**, 660.
30 G. S. Rushbrooke and P. J. Wood, *Mol. Phys.*, 1963, **6**, 409; M. E. Lines, *J. Phys. Chem. Solids*, 1970, **31**, 101.

Paper 9/03487K